Journal of
Applied
Crystallography
ISSN 0021-8898

Received 11 August 2009
Accepted 20 October 2009

Neutron powder diffraction in materials with incoherent scattering: an illustration of Rietveld refinement quality from nondeuterated gypsum

Paul F. Henry,[a]* Mark T. Weller[b] and Chick C. Wilson[c]

[a]Helmholtz Zentrum Berlin für Materialien und Energie GmbH, Hahn-Meitner-Platz 1, 14109 Berlin, Germany, [b]Chemistry School, University of Southampton, Highfield, Southampton SO171BJ, UK, and [c]Department of Chemistry, Joseph Black Building, University of Glasgow, Glasgow G128QQ, UK. Correspondence e-mail: paul.henry@helmholtz-berlin.de

The power of the state-of-the-art neutron powder diffractometer suite at the Institut Laue–Langevin for investigating the structure of nondeuterated materials is presented using gypsum, $CaSO_4{\cdot}2H_2O$, as a reference material. It is shown that flexible modern neutron powder diffraction instruments at reactor-based sources can yield data with sufficient counting statistics above the incoherent scattering contribution to perform unconstrained refinements in relatively short time periods (from minutes to a few hours, depending on the sample size and the instrument choice), without the requirement for significant changes to the standard operational modes of the instruments. The results are critically compared with previous literature from single-crystal and powder X-ray and neutron measurements on deuterated and nondeuterated gypsum.

1. Introduction

Traditionally, the collection of neutron powder data from hydrogenous materials is considered largely fruitless owing to the substantial incoherent scattering contribution from the hydrogen. This, coupled with relatively low neutron fluxes, leads to disproportionately long counting times for the quality of data collected. In fact, deuteration is almost seen as a prerequisite for a neutron powder experiment for these reasons. However, in many cases, deuteration profoundly changes the properties of the material under investigation (for instance, changes in ferroelectric transition temperatures are found for the classical alkali metal dihydrogen phosphates, *e.g.* KH_2PO_4), so that observations are in effect being made for a material with a completely different structure and phase behaviour as a function of a variable parameter (temperature, pressure *etc.*). In addition, deuteration can be expensive to perform for more complex materials, yielding much smaller sample volumes than are available for their hydrogenous analogues, which impacts negatively on counting times and data statistics. Often deuteration is incomplete or impossible and, because of the difference in the coherent neutron scattering lengths of hydrogen and deuterium (−3.7406 and 6.671 fm, respectively), incomplete deuteration can make the location of hydrogen more difficult by producing an effectively null- or near-to-null-scattering site. It is clear that implementation of methodology that allows routine hydrogen position definition from easily synthesized material [*i.e.* non-isotopically enriched, and in polycrystalline or small-single-crystal (< 50 μm) form] would be both of widespread application and of key importance.

In this manuscript, data are presented from the nondeuterated system gypsum, $CaSO_4{\cdot}2H_2O$, using the powder diffraction suite at the Institut Laue–Langevin (ILL) in order to illustrate that modern constant-wavelength neutron powder instruments can now address these problems and allow the study of hydrogenous polycrystalline materials. The manuscript concentrates on the data collection strategy and refinement methodology rather than the range of materials that could benefit from this approach, as the latter has been covered in detail elsewhere (Weller *et al.*, 2009). Data are presented from the instruments D20, D1A and D2B, and the instruments are critically compared. At 33 at% hydrogen, the incoherent contribution from the hydrogen to the background would have made this material almost impossible to study in acceptable timeframes with previous-generation neutron powder instruments, as implicitly stated in the previous published neutron powder studies on gypsum by Schofield *et al.* (1996) as their motivation for deuteration.

Gypsum, in its natural form, is an evaporite mineral most commonly found in layered sedimentary deposits in association with halite, anhydrite, sulfur, calcite and dolomite. It is the most common sulfate-based mineral in the world and, thanks to its peculiar constant bulk volume, dehydration and rehydration behaviour, has many uses in the building and casting industry, including manufacture of wallboard, cements and plaster of Paris and as a hardening retarder in Portland cement. Other uses span such diverse fields as dentistry (casts) and agriculture (soil conditioning). Other varieties of natural microcrystalline gypsum, such as ‘satin spar’ and ‘alabaster’, are used for a variety of ornamental purposes, although their low hardness limits durability. In the majority of the industrial

doi:10.1107/S0021889809043210

uses, the water content and its variation as a function of temperature drive the properties, and therefore a full understanding of the structure and water dynamics is fundamental.

The crystal structure of gypsum has been studied extensively in order to understand its structure in relation to its properties and industrial uses. The initial work using X-ray data by Wooster (1936) was supplemented by neutron data by Atoji & Rundle (1958) and further X-ray work by Cole & Lancucki (1974). Pedersen & Semmingsen (1982) used single-crystal neutron diffraction under ambient conditions to solve the structure and this remains the best structural model. Schofield *et al.* (2000) studied the material as a function of temperature, also using single-crystal neutron diffraction, to investigate the thermal properties of the hydrous components. A deuterated form of the natural mineral was also studied by Schofield *et al.* (1996) using neutron powder diffraction, which showed there was a minimal effect on the structure by replacing hydrogen by deuterium. The powder structure was also subsequently redetermined by Boeyens & Ichharam (2002) in order to confirm that synthetic and natural gypsum samples were identical structurally and to present the unit-cell contents in the standard *C*2/*c* space-group setting rather than the unconventional *I*2/*a* setting used by most of the previous authors.

The structure of gypsum, as illustrated in Fig. 1, is formed of layers linked by hydrogen bonding. The layers consist of zigzag chains of CaO_8 polyhedra in the **a** direction (in the nonstandard *I*2/*a* cell) bound by similar zigzag chains of SO_4^{2-} units. These double-sheet polyhedral layers are linked by the O1···H2 hydrogen bond. The important properties of gypsum in terms of its dehydration/rehydration are related to the presence and arrangement of the water molecules; interpretation of these properties is highly dependent on knowing accurately the complete structure, including hydrogen positions and bonding and anisotropic displacements as a function of temperature. To date, only single-crystal neutron diffraction data have been able to provide sufficient information to allow all of these studies to be carried out; for this system, large high-quality single crystals occur naturally or are easily prepared.

The fact that the structure is not significantly perturbed by substitution of deuterium for hydrogen makes gypsum an ideal candidate for a case study as the existing literature allows a critical comparison between the different data collection strategies (X-ray or neutron, powder or single crystal, hydrogenated or deuterated sample) to be performed. In addition, the unit-cell volume of around 500 Å^3 and the monoclinic space group (*C*2/*c*) are sufficiently complex to investigate how peak overlap in the one-dimensional powder diffractogram affects the derived standard uncertainties as a function of variables such as counting time and sample size.

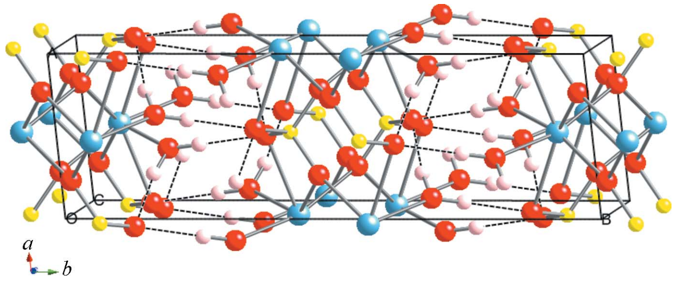

Figure 1
The crystal structure of gypsum in the space group *C*2/*c*, illustrating the layers bound by hydrogen bonding. The Ca atoms are light blue, the H atoms are pink, S yellow and O red. The hydrogen bonds are shown as dashed lines.

2. Experimental

For this study, samples from a single batch of $CaSO_4 \cdot 2H_2O$ (98% American Chemical Society specification from Aldrich; < 0.02% K, Mg *etc.*; < 0.05% Sr) were used. Boeyens & Ichharam (2002) have shown that synthetic and natural samples of gypsum are structurally identical. The purity of the material was checked by X-ray powder diffraction using a Bruker D8 ADVANCE diffractometer operating in Bragg–Brentano geometry with a primary-beam graphite monochromator and Cu $K\alpha_1$ radiation (λ = 1.5406 Å). The water content and decomposition products were verified by thermogravimetric analysis (TGA) using a Polymer Laboratories STA1500 DTA/TGA balance in flowing air. The sample was heated at a rate of 1 K min^{-1} from room temperature to 773 K, held for 30 min at this temperature and then cooled back to room temperature at 10 K min^{-1}.

For the neutron powder diffraction experiments, samples were prepared from the single characterized batch of gypsum and loaded into the standard cylindrical vanadium cans used at the ILL, with external diameters ranging from 5–9 mm (five samples) to more than the full beam height; the largest is approximately 40 mm with the chosen configuration at D20. Thus the sample volumes ranged from 0.7 to 2.3 cm^3 and the sample masses from 0.75 to 3.0 g, which is around 50% of the measured density of 2.3 g cm^{-3} as a result of using powdered samples rather than pressed pellets and non-ideal packing of all powdered materials. This also allowed absorption corrections and sample attenuation to be determined for each sample using the standard cylindrical geometry calculation [Rouse *et al.*, 1970; *International Tables for Crystallography*, (1992), Vol. C, p. 250]. All data collections were performed at room temperature in order to minimize the background contributions from sample environment and to aid the comparative studies, as the majority of the data were collected at around room temperature, though the advantages of measuring at low temperature to maximize the signal-to-background are acknowledged for hydrogenous materials [see Weller *et al.* (2009) for more details].

The D20 high-flux two-axis diffractometer has undergone a number of upgrades in recent years since the preliminary reports (Hansen, 2004; Convert *et al.*, 1998, 2000), and the current instrument characteristics are summarized in the ILL *Yellow Book* (Cicognani, 2005). The most relevant upgrade for this work was the commissioning of the high-takeoff-angle, so-called 'high-resolution', configuration using a Ge(113) cut-surface single-crystal monochromator as detailed in the recent manuscript by Hansen *et al.* (2008). In fact, the observed instrumental resolution function for the high-takeoff-angle configuration is very similar to that for the high-resolution instrument D2B in its highest-flux setting but with a relative speed 25–30 times faster than this instrument, as the full scattering angle is collected in real time. Therefore, D20 addresses all of the concerns outlined in the introduction limiting the investigation of hydrogenous materials, as it has both a continuous high incident-neutron flux with a large, high-efficiency area detector (*i.e.* fast data collection with high count rates) and good resolution over a large Q range for structural refinements (*i.e.* the FWHM does not significantly change across the majority of the detector).

Air scattering was reduced by placing the sample in an evacuated bell-jar and the instrumental contribution to the background minimized by choosing sample slits such that the beam at the sample position was no more than 0.5 mm wider than the vanadium can. The incident beam Soller collimation was set in the open position (27′ natural beam divergence) in order to maximize the flux at the sample position. Data were collected at two wavelengths, 1.87 and 1.36 Å, which were calibrated using a NIST silicon sample (SRM640b) using identical conditions to those of the experiment. Data were collected in 300 s time slices at both wavelengths for each sample size until well after the point at which Rietveld refinements showed saturation of the counting statistics (determined as the point where standard uncertainties become effectively constant) and then normalized and corrected for the individual detector efficiencies using the ILL in-house software suite *LAMP* (Richard *et al.*, 1996; http://www.ill.Fr/data_treat/lamp/lamp.html).

The setups used for D1A and D2B were those as summarized in the ILL *Yellow Book* (Cicognani, 2005). Only the 9 mm sample can was used because of the much longer counting times required. Data were collected on D1A at 1.909 and 1.4 Å, calibrated using the NIST silicon sample. Step scans were performed using a 0.05° step size to give a full scan every 2 h, up to 14 h at 1.909 Å and 12 h at 1.4 Å. For D2B, data were collected under the highest flux conditions at 1.594 and 1.23 Å (20′ pre-monochromator Soller slits and 250/250 post-monochromator slits), also calibrated using the NIST 640b silicon sample, with a sample window on the $\alpha 2$ optics (optics between the monochromator and the sample) such that the incident beam size at the sample position was 50 mm high by 12 mm wide. Step scans were performed using a 0.05° step size to give a full block of eight scans every hour up to 4 h at 1.594 Å and every 1.5 h up to 6 h at 1.23 Å. The data were normalized for the detector efficiencies using *LAMP* and data files created for both the middle 10 cm of the detectors (highest resolution) and the whole 30 cm height of the detectors (highest count rate) for comparative refinements. D1B, the fourth powder instrument in the thermal suite of instruments at ILL, was not used; its instrument characteristics are not suitable for full structural refinement across large Q ranges, as a result of the low monochromator takeoff angle, limited area-detector angle coverage and insufficient angular resolution.

For each instrument and wavelength, the data were initially normalized into single data sets – 300 s for D20, 1 h for D2B and 2 h for D1A. Further incremental time data sets were generated by combining the individual data sets, with full error propagation analysis, to give single files of variable data collection time. Thus, both the evolution of the statistical errors with time and the stability of the instruments could be probed simultaneously with the chosen data strategy. Rietveld analysis was carried out using the *GSAS* suite of programs (Larson & Von Dreele, 1994) using both *EXPGUI* (Toby, 2001) for manual refinement and *PC-GSAS* batch mode in order to probe the robustness of the refined global minima from the individual data sets. Initially, refinements were performed using single-wavelength data on D20 for each sample size, and subsequently multi-wavelength refinements were carried out for all of the instruments used for comparison. All of the Rietveld refinements were carried out with the use of no soft constraints on bond lengths or angles in order to critically compare the powder instruments used with the previously published data.

3. Results

The format of the presentation of the results is as follows: raw data analysis investigating the counting statistics, stability and repeatability of the data collections, Rietveld refinements of the D20 data compared with the previous literature, and, finally, a critical comparison of the other ILL instruments with D20. As the subject of this manuscript is the application of the ILL thermal neutron instruments to the investigation of the nondeuterated material, the pre-neutron sample characterization information (powder X-ray diffraction, TGA) have been deposited as supplementary information[1] and will not be discussed here. However, the measurements show that the material is high purity and that the water content is fully stoichiometric, allowing the published models to be used as the basis for the refinements.

3.1. Raw data analysis

Fig. 2 shows typical 300 s data collections from gypsum for an 8 mm sample on D20 at the two wavelengths studied. At 33 at% hydrogen, the incoherent scattering contribution is significant and the ratio of the most intense peak from the gypsum to the level of the background is around 1:1. Fig. 3 shows patterns collected under a range of total counting times in the mid-Q region of 5.6–6.3 Å^{-1}. It is clear from Fig. 3 that the background is well defined as a function of scattering angle, even at the highest Q measured (6.3 Å^{-1} is equivalent to around 140° scattering angle with an incident wavelength of 1.87 Å), and can be easily modelled by a simple function. In order to extract the accurate integrated intensities for individual Bragg reflections, which is the requirement for a good Rietveld refinement from powder data, it is crucial to have

---

[1] Supplementary material is available from the IUCr electronic archives (Reference: CG5117). Services for accessing these data are described at the back of the journal.

well resolved Bragg reflections wherever possible (*i.e.* to minimize overlap) and a well defined instrumental peak shape. Often overlooked is the fact that there is also the requirement that the background itself be well defined with low noise, as this is also crucial for the extraction of accurate integrated intensities, particularly when peak overlap is significant, as becomes the case at higher scattering angles or when the complexity of the material is increased. In general, a low background when compared with the peak intensity gives reliable integrated intensities, whereas a high background gives poorly defined integrated intensities, leading to higher standard uncertainties on the refined structural variables. It is this point that has led to the prevalent view that high-background data sets always give poor integrated intensities. Fig. 3 clearly shows that the inherent noise level of the background is very low, even at the highest Q, because of the high count rate and detector stability, even though the absolute intensity of the background is high.

The effect of the sample size on the count rate was followed by measuring 300 s data sets on each of the five sample cans (5–9 mm external diameter cylinders) with the beam size optimized for the sample size in each case. In order to optimize the beam size, a fixed slit width incident beam was scanned perpendicular to the sample to define the beam centre. The left and right sample slits were then opened progressively until the intensity of the Bragg reflections became constant with respect to the background, *i.e.* full illumination of the sample. The volumes of the samples were recorded along with the mass so that the effective packing density of each sample could also be determined. Fig. 4(*a*) shows the raw data as a function of the sample size and Fig. 4(*b*) shows the data normalized to the most intense peak.

The importance of these measurements is that secondary scattering events (multiple scattering, absorption *etc.*) within

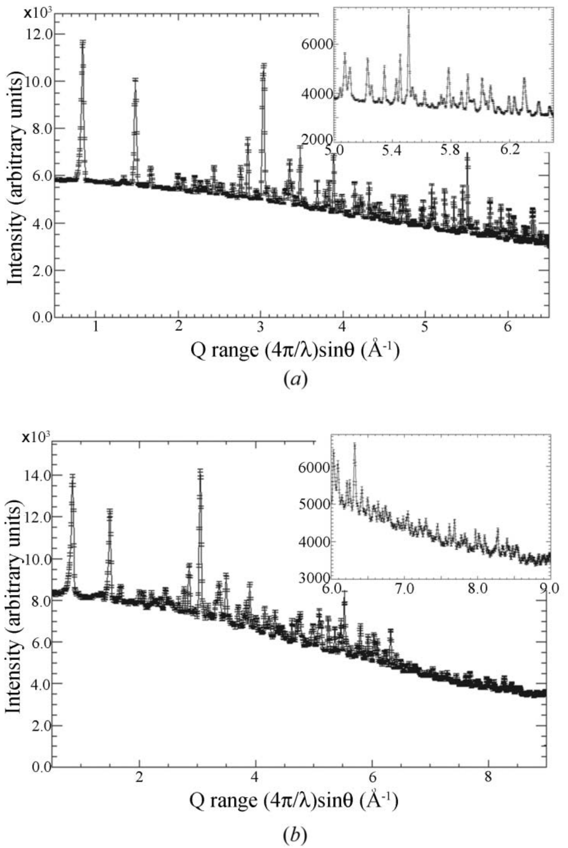

Figure 2

Typical 300 s data sets with error bars from a 9 mm can sample of gypsum collected using D20 and an incident wavelength of 1.87 Å (*a*) and 1.36 Å (*b*) as a function of Q with the high Q region inset in each case.

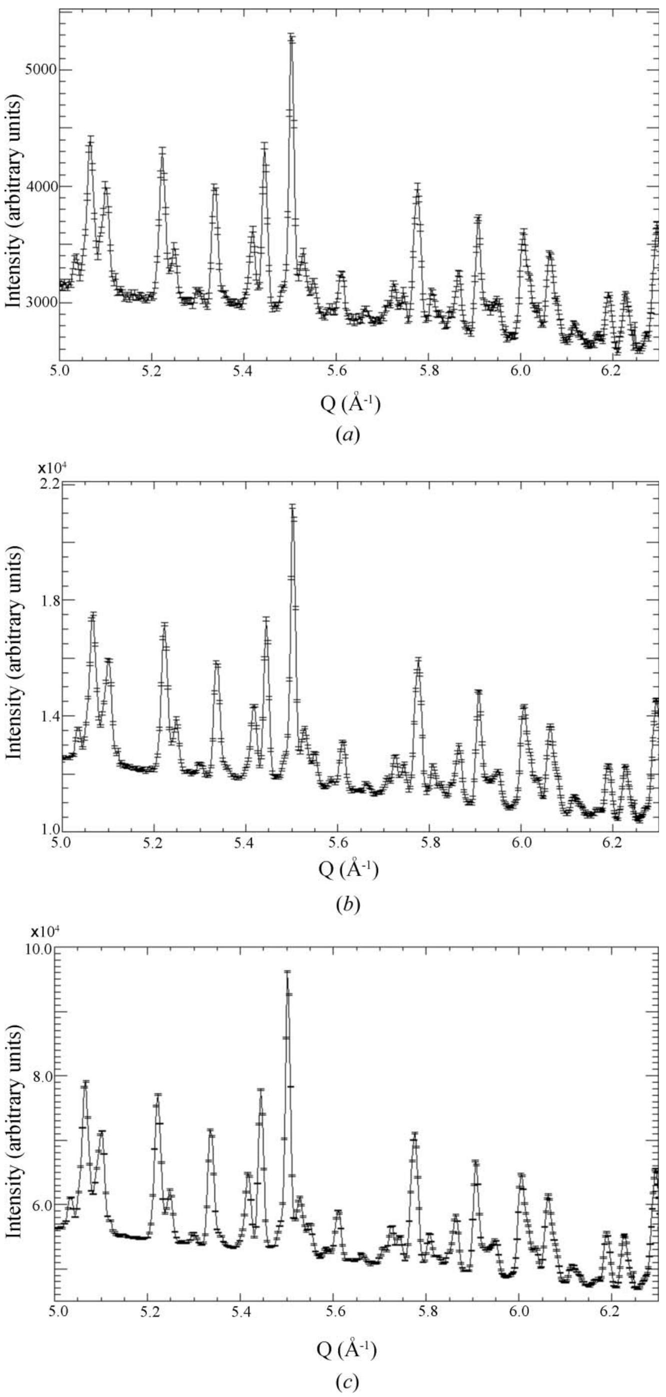

Figure 3

Raw data sets from the 9 mm sample of gypsum with counting times of 5 min (*a*), 20 min (*b*) and 90 min (*c*) in the Q region of 5.0–6.3 Å^{-1}, illustrating the evolution in the signal-to-noise ratio.

Table 1
Refined lattice constants and volume as a function of sample size from D20 data.

Sample size	a (Å)	b (Å)	c (Å)	β (°)	Volume (Å^3)
5 mm	6.28581 (15)	15.2097 (4)	6.52888 (16)	127.4300 (9)	495.673 (22)
6 mm	6.28556 (15)	15.2098 (4)	6.52849 (16)	127.4292 (9)	495.629 (21)
7 mm	6.28603 (14)	15.2102 (4)	6.52889 (15)	127.4291 (9)	495.712 (21)
8 mm	6.28662 (14)	15.2106 (4)	6.52938 (15)	127.4307 (9)	495.799 (21)
9 mm	6.28636 (14)	15.2107 (4)	6.52914 (15)	127.4273 (10)	495.784 (21)

the sample should become an increasingly important factor as the sample size increases, leading to an overall increase in the background with respect to the Bragg peak intensity. The effect would be to offset the position of the averaged centre of scattering (reaching the detector) within the sample — *i.e.* it would no longer be the centre of the sample but displaced towards the detector side of the sample. This should lead to a measurable change in the observed peak shapes and their positions, particularly at high scattering angles, as the sample size is increased and gives changes in the refined lattice constants that cannot be accounted for by a simple change in refined zero point. For a more detailed explanation of this effect see Langford & Louer (1996) and references therein. Table 1 gives the extracted lattice parameters as a function of sample size for comparison; the variance is less than 0.04% across the five samples and there is no evidence of a systematic change as the sample size is increased. Fig. 4(*b*) shows that there is a small increase in the background contribution for the 9 mm sample (of the order of a few percent) compared with the other sample can sizes but for the majority of the sample sizes there is no measurable effect – *i.e.* the peak-to-background ratio remains constant when the data sets are normalized to the maximum peak intensity. The larger background contribution for the 9 mm sample is constant as a function of scattering angle and may be non-sample scattering, such as that from the solid vanadium foot of the sample can; there is no evidence of an increase in the FWHM of the reflections at fixed scattering angle as a function of sample size.

In the present study, only a single sample composition was used, and so it has not been possible to investigate directly the effect of the hydrogen content on the measured signal/background/noise ratio. In addition, the packing density of the powdered sample relative to the measured single-crystal density will also have a significant influence on the impact of multiple scattering and beam attenuation in a diffraction experiment. For samples having higher hydrogen contents, such as clathrates and hydrides (~65–75 at%), theory predicts that annular sample cans should be employed, as used for materials with high beam absorption (Schmitt & Ouladdiaf, 1998), though true absorption and the attenuation effect caused by the hydrogenous incoherent scattering are not identical. However, it is clear from our results that for hydrogen-containing powder materials measurements do not support this hypothesis, showing that even in extreme cases larger sample volumes give better results (Kuhs, 2008). Such deviation from theory can be explained by the low packing densities of powders compared with the ideal single-crystal or liquid densities that are used in the calculations. As powdering the sample will often reduce the density to less than 50% of the ideal single-crystal value, the effect is similar to diluting a sample with a matrix, another technique often used with strongly absorbing materials. This effect will be further studied as part of the accepted instrument development work at ILL in 2009–2010 as it is likely to have important implications for broader use of powder diffraction techniques for hydrogenous materials.

3.2. Rietveld analysis

3.2.1. D20 structural refinements. The initial models for the refinements were taken from the work of Schofield *et al.* (1996) for the $I2/a$ model and Boeyens & Ichharam (2002) as listed by the ICSD database (Bergerhoff & Brown, 1987; Belsky *et al.*, 2002) for the space group $C2/c$. A six-term cosine Fourier series was refined for the background and no constraints were placed on any refined parameter. Anisotropic atomic displacement parameters (ADPs) were refined in all

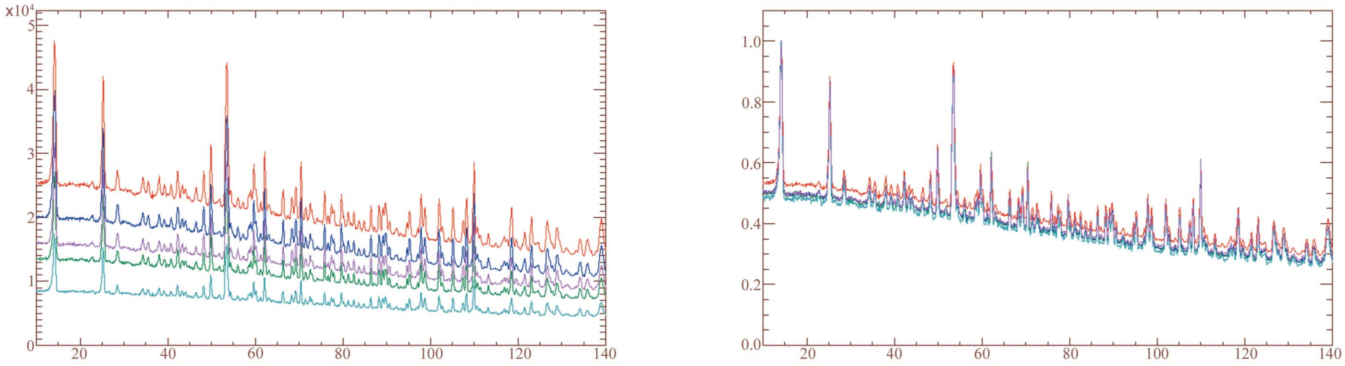

(*a*) (*b*)

Figure 4
(*a*) Raw data as a function of scattering angle with 1.87 Å incident neutron wavelength, showing the effect of increasing the sample size from 5 to 9 mm. (*b*) The data normalized to the most intense peak in order to illustrate the evolution of the background contribution with increasing sample size. In each case the light blue line represents the 5 mm sample, green the 6 mm sample, magenta the 7 mm sample, dark blue the 8 mm sample and red the 9 mm sample data.

Table 2
Refined atomic coordinates for gypsum from various data collection types and strategies.

(CW) is continuous wavelength data, (t.o.f.) is time of flight data, (H) is using the hydrogenated material and (D) is the deuterated material. Unless otherwise stated, the space group is the nonstandard *I*2/*a* cell.

Atom	Neutron powder (CW) (H)†	Neutron powder (t.o.f.) (D)‡	Single-crystal neutron (t.o.f.) (H)§	Single-crystal neutron (CW) (H)¶	Single-crystal X-ray (H)††	Single-crystal X-ray *C*2/*c* (H)‡‡	Neutron powder *C*2/*c* (CW) (H)†
Ca							
x	0.5	0.5	0.5	0.5	0.5	0.5	0.5
y	0.07872 (29)	0.07864 (32)	0.078983 (15)	0.07967 (9)	0.07970 (10)	0.079556 (14)	0.07854 (27)
z	0.25	0.25	0.25	0.25	0.25	0.75	0.75
S							
x	0.0	0.0	0.0	0.0	0.0	0.0	0.0
y	0.0775 (4)	0.07872 (42)	0.0773 (2)	0.07705 (13)	0.07720 (10)	0.077240 (16)	0.0774 (4)
z	0.75	0.75	0.75	0.75	0.75	0.75	0.75
O1							
x	0.9649 (4)	0.96164 (50)	0.9640 (3)	0.96320 (15)	0.9607 (3)	0.03721 (14)	0.0353 (4)
y	0.13261 (16)	0.13263 (15)	0.13211 (10)	0.13190 (5)	0.1312 (1)	0.13198 (5)	0.13257 (14)
z	0.5519 (4)	0.55120 (43)	0.5506 (2)	0.55047 (13)	0.5518 (2)	0.58718 (13)	0.5871 (4)
O2							
x	0.7572 (4)	0.75714 (48)	0.7575 (2)	0.75822 (15)	0.7592 (2)	0.24239 (13)	0.2426 (4)
y	0.02286 (17)	0.02154 (18)	0.02218 (10)	0.02226 (5)	0.0227 (1)	0.02211 (4)	0.02279 (15)
z	0.6674 (4)	0.66527 (39)	0.6669 (2)	0.66709 (13)	0.6661 (2)	0.90917 (13)	0.9101 (4)
O (H_2O)							
x	0.3808 (6)	0.37837 (60)	0.3817 (3)	0.37960 (21)	0.3778 (3)	0.62022 (19)	0.6191 (5)
y	0.18264 (20)	0.18255 (21)	0.18219 (11)	0.18212 (7)	0.1820 (1)	0.18197 (5)	0.18253 (18)
z	0.4569 (5)	0.46544 (54)	0.4603 (3)	0.45881 (16)	0.4588 (2)	0.07844 (16)	0.0763 (5)
H1							
x	0.2486 (9)	0.25043 (64)	0.2508 (7)	0.25112 (41)	–	0.749 (3)	0.7512 (8)
y	0.15985 (28)	0.16150 (20)	0.1615 (3)	0.16158 (11)	–	0.1619 (14)	0.16020 (26)
z	0.5068 (9)	0.50086 (61)	0.5070 (7)	0.50372 (35)	–	0.251 (4)	0.2578 (8)
H2							
x	0.4067 (10)	0.40225 (69)	0.4069 (7)	0.40458 (36)	–	0.584 (5)	0.5936 (9)
y	0.24186 (37)	0.24347 (20)	0.2435 (2)	0.24275 (13)	–	0.2351 (19)	0.24203 (34)
z	0.4937 (10)	0.49003 (61)	0.4926 (7)	0.49217 (31)	–	0.073 (5)	0.0872 (9)

† This work 300 K. ‡ Schofield *et al.* (1996), 320 K. § Schofield *et al.* (2000), 200 K. ¶ Pedersen & Semmingsen (1982), 294 K. †† Cole & Lancucki (1974), 300 K. ‡‡ Boeyens & Ichharam (2002), 293 K.

cases. Fig. 5 shows the final fit to the Rietveld refinement of the 9 mm gypsum sample can data after 90 min collection time using the nonstandard space group *I*2/*a* model for one of the wavelengths. Table 2 shows the refined atomic positions compared with those from the previous single-crystal and powder studies on both the hydrogenous and deuterated materials with the associated references and data collection temperatures. The CIF data for both of the possible space-group models, and plots of the Rietveld refinement fits and fit statistics for each measured wavelength, have been deposited as supplementary information.

The positions and standard uncertainties for the powder data on the hydrogenated and deuterated materials are in good agreement, showing that there is no significant isotope effect in this material, as required for this comparative study. As one of the main reasons for Schofield *et al.* choosing to study the deuterated material was the incoherent contribution from hydrogen to the background, the close agreement for data collected for 90 min on D20 using the hydrogenous material and approximately 2 h on the POLARIS diffractometer at ISIS (350 μAh) using the deuterated sample shows the power of upgraded instrumentation in overcoming the drawbacks of investigating hydrogen-containing materials.

In order to overcome the difficulty of directly comparing the single-crystal X-ray data and the neutron powder data, due to the different space-group choices of Boeyens & Ichharam and Cole & Lancucki, Table 2 also contains the results from the same data presented in Fig. 5 refined using the *C*2/*c* model. The definition of the high atomic number elements is to a higher precision than the powder data but is significantly

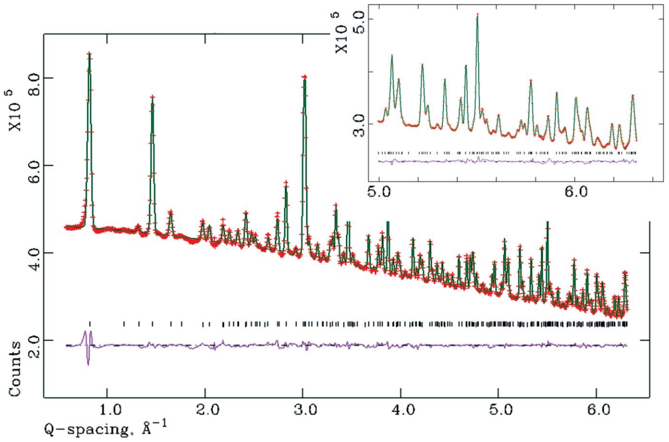

Figure 5
Final Rietveld refinement profile for the 1.87 Å incident wavelength data for the 9 mm sample can of gypsum. The observed data are crosses, the calculated pattern a solid line, the tick marks show the allowed reflections and the lower solid line is the difference plot; R_{wp} = 1.78%, R_p = 0.92% and R_{F^2} = 4.78% for 273 observations. The inset shows the higher *Q*-space region.

Table 3
Anisotropic atomic displacement parameters (Å^2 × 100).

Continuous-wavelength single-crystal data at 294 K.

	U_{11}	U_{22}	U_{33}	U_{12}	U_{13}	U_{23}
Ca	2.07 (8)	2.58 (8)	1.95 (8)	0	0.81 (6)	0
S	1.90 (11)	2.04 (10)	1.92 (11)	0	0.86 (10)	0
O1	2.62 (4)	2.79 (4)	2.43 (4)	−0.11 (4)	1.23 (3)	0.44 (3)
O2	2.22 (4)	2.70 (4)	2.54 (3)	−0.46 (4)	0.92 (3)	0.08 (3)
O(H_2O)	3.91 (5)	2.94 (6)	3.91 (5)	0.01 (5)	2.53 (4)	−0.38 (4)
H1	5.99 (19)	4.64 (9)	6.32 (10)	−0.12 (9)	4.32 (9)	0.18 (8)
H2	5.96 (10)	3.83 (9)	7.14 (11)	−0.39 (11)	3.84 (9)	−0.85 (10)

Time-of-flight single-crystal data at 200 K.

	U_{11}	U_{22}	U_{33}	U_{12}	U_{13}	U_{23}
Ca	0.53 (7)	0.42 (8)	0.49 (7)	0	0.22 (4)	0
S	0.09 (10)	0.33 (12)	0.33 (11)	0	0.03 (10)	0
O1	0.68 (4)	0.85 (5)	0.77 (5)	−0.08 (4)	0.31 (4)	0.26 (5)
O2	0.38 (4)	0.82 (5)	0.72 (5)	−0.28 (4)	0.13 (4)	0.04 (5)
O(H_2O)	1.63 (7)	1.01 (6)	1.80 (7)	−0.03 (5)	1.20 (6)	−0.22 (6)
H1	3.43 (15)	2.76 (16)	3.53 (16)	−0.30 (13)	2.89 (14)	0.01 (16)
H2	3.80 (16)	1.59 (13)	4.23 (18)	−0.34 (12)	2.40 (15)	−0.68 (16)

This work, using the hydrogenated powdered material at 300 K.

	U_{11}	U_{22}	U_{33}	U_{12}	U_{13}	U_{23}
Ca	1.36 (20)	1.32 (22)	0.86 (19)	0	1.08 (18)	0
S	0.31 (31)	0.92 (34)	1.27 (32)	0	0.37 (30)	0
O1	0.97 (7)	2.14 (13)	1.33 (11)	0.02 (10)	0.79 (9)	0.75 (9)
O2	0.56 (10)	2.21 (13)	1.61 (13)	0.38 (11)	0.60 (10)	0.64 (10)
O(H_2O)	2.22 (14)	2.50 (18)	1.28 (15)	0.66 (14)	0.71 (12)	0.18 (12)
H1	3.24 (24)	3.96 (33)	1.04 (20)	0.08 (22)	0.17 (20)	0.24 (22)
H2	3.96 (27)	3.81 (33)	3.81 (28)	0.00 (32)	1.86 (26)	−0.99 (30)

worse for the hydrogen positions, illustrating the inherent drawback of using X-ray diffraction methods to locate hydrogen in the presence of even moderate *Z* elements. In fact, Cole & Lancucki were not able to extract the hydrogen positions from their data, and the standard uncertainties for the more recent Boeyens & Ichharam data are an order of magnitude larger than those found in this study and for the single-crystal neutron investigations. As gypsum is not very complex (< 500 Å^3 and monoclinic) and does not contain very high atomic number elements, this is a significant result for the powder technique, especially when coupled with the use of a fully hydrogenated sample. Finally, comparison of the refined model in the *I*2/*a* space group in this work with those from the two published single-crystal neutron studies shows the refined standard uncertainties are 2–3 times larger than those found for the constant-wavelength data and 1–2 times larger than those found from the time-of-flight work. Taking into account the significant reduction in counting times for the powder investigation and the ease of sample preparation and mounting compared with a standard single-crystal neutron study, where large crystals are required, these results show that excellent precision can be obtained with powder data. In addition, the absolute values of the positional parameters are in good agreement with the single-crystal neutron investigations, showing that good accuracy can also be achieved with the powder method.

Direct comparison of the refined anisotropic displacement parameters from each of the respective works is difficult because of the different temperatures used for data collection and the fact that several of the works only list either isotropic or partial anisotropic atomic displacement parameter information. Table 3 shows the refined anisotropic atomic displacement parameters from this work compared with the constant-wavelength (Pedersen & Semmingsen, 1982) and time-of-flight (Schofield *et al.*, 2000) single-crystal neutron diffraction studies. A discussion of the anisotropic atomic displacements obtained with the time-of-flight and the constant-wavelength single-crystal data was presented by Schofield *et al.* (2000); while the absolute values of the refined parameters cannot be easily compared, because of the different data collection temperatures, the oblate forms of the displacement ellipsoids of the water molecule are consistent across all temperature ranges from 4.2 to 300 K, which is supported by the nondiffraction experiments (Seidl *et al.*, 1969; Berenblut *et al.*, 1973; Krishnamurthy & Soots, 1971; Winkler & Hennion, 1994). The H-atom ellipsoids are oriented such that the long direction is perpendicular to the direction of the hydrogen bond. The H-atom ellipsoids refined from the neutron powder data in this work have the same shape as those from the single-crystal data, although to a lower level of precision and accuracy, which is an unsurprising result as determination of the absolute values of the anisotropic atomic displacement parameters from powder data alone is notoriously unreliable. However, the fact that the shape of the ellipsoids matches those from the single-crystal data shows that the refinement of the powder data is robust.

Extraction of the bond lengths from the powder data refinement presented here shows that the bond lengths are 1.007 (6) and 0.929 (7) Å for O—H1 and O—H2, respectively, with a bond angle of 107.2 (5)°; these values compare favourably with those of 0.959 (3) Å, 0.942 (3) Å and 107.5 (2)°, respectively, obtained from the single-crystal neutron data of Schofield *et al.* (2000) at 294 K and 0.961 (6) Å, 0.948 (4) Å and 107.2 (5)° from the powder data on the deuterated material of Schofield *et al.* (1996) at 320 K. It should be noted that, in the latter work, the atomic displacement parameters were modelled isotropically, which can affect the derived bond lengths where there is significant transverse motion. The apparent increased variance of the absolute values for the bond lengths of the water molecule from this powder study compared with the previous single-crystal and powder study on the deuterated material is discussed below. Indeed, it is difficult to obtain a self-consistent set of atomic and displacement parameters owing to the differences in the origins of the scattering and potential systematic errors specific to one technique (for example, the choice of background position in analysis of powder diffraction data). This can be particularly evident in combined studies using X-ray and neutron data sets and is discussed further by Weller *et al.* (2009). The water molecules in gypsum are known to be significantly distorted from the ideal geometry in free water molecules from the previous work of Seidl *et al.* (1969) using infra-red spectroscopy, and so the

Table 4
Final atomic positions from the Rietveld refinements to investigate the effect of the choice and level of the background on the extracted parameters.

A description of each set of refinements is given in the text.

Atom	(1)	(2)	(3)	(4)	(5)	(6)	(7)
Ca							
x	0.5	0.5	0.5	0.5	0.5	0.5	0.5
y	0.07854 (27)	0.07842 (28)	0.0796 (4)	0.07846 (29)	0.0787 (4)	0.07854 (27)	0.07853 (27)
z	0.75	0.75	0.75	0.75	0.75	0.75	0.75
S							
x	0.0	0.0	0.0	0.0	0.0	0.0	0.0
y	0.0774 (4)	0.0763 (4)	0.0775 (7)	0.0763 (4)	0.0768 (6)	0.0773 (4)	0.0774 (4)
z	0.75	0.75	0.75	0.75	0.75	0.75	0.75
O1							
x	0.0353 (4)	0.0363 (4)	0.0347 (6)	0.0362 (4)	0.0346 (6)	0.0353 (4)	0.0353 (4)
y	0.13257 (14)	0.13188 (16)	0.13252 (24)	0.13188 (16)	0.13278 (23)	0.13259 (14)	0.13258 (14)
z	0.5871 (4)	0.5865 (4)	0.5869 (6)	0.5863 (4)	0.5867 (6)	0.5871 (4)	0.5871 (4)
O2							
x	0.2426 (4)	0.2419 (4)	0.2415 (6)	0.2420 (4)	0.2424 (6)	0.2427 (4)	0.2426 (4)
y	0.02279 (15)	0.02226 (17)	0.02235 (24)	0.02222 (17)	0.02308 (22)	0.02280 (15)	0.02279 (15)
z	0.9101 (4)	0.9099 (4)	0.9096 (6)	0.9099 (4)	0.9095 (6)	0.9101 (4)	0.9101 (4)
O(H_2O)							
x	0.6191 (5)	0.6209 (5)	0.6257 (7)	0.6209 (6)	0.6176 (9)	0.6192 (5)	0.6191 (5)
y	0.18253 (18)	0.18199 (19)	0.18408 (28)	0.18187 (20)	0.18243 (28)	0.18250 (18)	0.18253 (18)
z	0.0763 (5)	0.0779 (5)	0.0788 (7)	0.0778 (5)	0.0745 (10)	0.0763 (5)	0.0763 (5)
H1							
x	0.7512 (8)	0.7520 (10)	0.7506 (14)	0.7520 (10)	0.7522 (13)	0.7512 (8)	0.7512 (8)
y	0.16020 (26)	0.16076 (33)	0.1608 (5)	0.16071 (35)	0.1603 (4)	0.16014 (26)	0.16020 (26)
z	0.2578 (8)	0.2563 (9)	0.2533 (14)	0.2564 (10)	0.2592 (12)	0.2578 (8)	0.2578 (8)
H2							
x	0.5936 (9)	0.5935 (10)	0.5943 (14)	0.5929 (11)	0.5944 (15)	0.5936 (9)	0.5936 (9)
y	0.24203 (34)	0.24220 (36)	0.2397 (5)	0.24254 (38)	0.2423 (5)	0.24217 (34)	0.24203 (34)
z	0.0872 (9)	0.0843 (9)	0.0780 (11)	0.0839 (10)	0.0885 (15)	0.0874 (9)	0.0872 (9)

bond-length mismatch between O—H1 and O—H2 is not unexpected. This is caused by a stronger hydrogen bond between H1 and the framework (see Fig. 1), as O—H1 is involved in an intra-layer hydrogen bond whereas O—H2 forms an inter-layer hydrogen bond and so is likely to be much weaker at 300 K.

Further refinements were carried out on the powder data from the 9 mm sample in order to determine the effect of the calculated background position and *Q* range on the extracted atomic parameters and ADPs. In all cases, a cosine Fourier series background with six terms was used; refinements were carried out as detailed below and the results are summarized in Tables 4–6:

(1) Refined background using both wavelength data sets (as presented in Tables 2 and 3).

(2) Only the large *Q* range data (λ = 1.36 Å) with a manually chosen background fixed to the fitted values.

(3) As (2), but with the manual background points chosen to be lower by around 5% at high *Q*.

(4) As (3), but in the final set of cycles the background was allowed to vary.

(5) Only the limited *Q* range data (λ = 1.87 Å) with a manually fixed background.

(6) As (4), but containing both wavelength data sets with the background for the limited *Q* range data fixed as in (5).

(7) As (6), but background now allowed to vary [identical conditions to (1) but approached from a different refinement route].

It is clear that, for the data covering larger values of *Q*, the background level has a significant effect on the extracted parameters. Comparison of the results from refinements of type (2) with those of type (5) (identical refinement variables) shows that the larger *Q* range data have higher precision and accuracy on the refined atomic variables, the expected result. It is significant that the results from refinement (3) are much poorer than those of either type (2) or (4), and that there are large changes in the positions and ADPs of the refined H-atom positions and the geometry of the interlayer water molecules. This indicates that a poor background choice in refinements of hydrogenous materials at longer *Q* will greatly influence the refined parameters. Therefore, in the cases of very high peak overlap at high *Q*, great care must be taken to ensure that the background level is realistic, otherwise parameter correlation becomes important. This is true for all powder data, but for highly crystalline materials with very high peak-to-background ratios the effects on the refined parameters in Rietveld analysis are very small. The degree of peak overlap at high *Q* also determines the maximum complexity of the hydrogen-containing structure that can be tackled using this technique for any given hydrogen content. The robustness of the results of the refinements is also illustrated well by the fact that refinements (1) and (7) yield identical results, even though the starting models and the order of refinement of the variables for each were different. The very small differences in the refined values for the variables of types (2) and (4) (carefully chosen fixed manual background *versus* refined background) show that this system is well within the complexity limit, as there is little serial correlation between the background parameters and the atomic variables. Finally, comparison of the refinements of types (2) and (4) (single wavelength covering large *Q*) with (1) and (7) (multi-wavelength) show that there is some disparity in the O—H bond lengths and angles. The multi-wavelength data show a difference of 0.02 Å in one of the water bond lengths and a 1° decrease in the H1—O—H2 bond angle. This mismatch is thought to be a result of the variation of the incoherent scattering cross section of hydrogen as a function of the incident wavelength, which in very simplistic terms could be described as a requirement for a different absorption correction for each constant-wavelength data set. This issue, albeit small in this material, requires further investigation; it is likely to have a serious impact on analysis of time-of-flight data from hydrogenous materials because the attenuation/absorption from the sample will be both energy/wavelength dependent and detector-angle dependent owing to the change in the average path length of a scattered neutron through the sample.

Table 5
Final anisotropic atomic displacement parameters (Å^2 × 100) from the Rietveld refinements to investigate the effect of the choice and level of the background on the extracted parameters.

A description of each set of refinements is given in the text.

ADP	(1)	(2)	(3)	(4)	(5)	(6)	(7)
Ca							
U_{11}	1.36 (20)	0.77 (16)	−0.47 (20)	0.75 (17)	1.6 (4)	1.41 (20)	1.35 (20)
U_{22}	1.32 (22)	1.96 (23)	2.46 (35)	1.94 (24)	1.3 (4)	1.37 (22)	1.32 (22)
U_{33}	0.86 (19)	1.23 (18)	−0.45 (21)	1.22 (19)	0.43 (33)	0.87 (19)	0.87 (19)
U_{12}	0	0	0	0	0	0	0
U_{13}	1.08 (18)	0.77 (15)	−0.52 (18)	0.75 (15)	1.00 (33)	1.09 (18)	1.07 (18)
U_{23}	0	0	0	0	0	0	0
S							
U_{11}	0.31 (31)	0.09 (23)	0.0 (4)	0.06 (25)	1.0 (6)	0.44 (31)	0.31 (31)
U_{22}	0.92 (34)	2.0 (4)	3.6 (7)	2.0 (4)	0.8 (6)	0.83 (34)	0.91 (32)
U_{33}	1.27 (32)	1.00 (26)	0.2 (4)	1.00 (27)	1.6 (6)	1.39 (32)	1.28 (32)
U_{12}	0	0	0	0	0	0	0
U_{13}	0.37 (30)	0.39 (24)	0.3 (4)	0.38 (25)	0.5 (6)	0.49 (29)	0.36 (30)
U_{23}	0	0	0	0	0	0	0
O1							
U_{11}	0.97 (9)	0.91 (9)	−0.17 (12)	0.88 (9)	0.92 (15)	0.98 (9)	0.96 (9)
U_{22}	2.14 (13)	2.68 (14)	2.98 (23)	2.66 (15)	2.04 (19)	2.14 (13)	2.14 (13)
U_{33}	1.33 (11)	1.39 (11)	0.38 (15)	1.38 (12)	1.29 (17)	1.36 (11)	1.33 (11)
U_{12}	0.02 (10)	0.27 (10)	−0.49 (13)	0.29 (10)	−0.14 (16)	0.02 (10)	0.02 (10)
U_{13}	0.79 (9)	0.77 (9)	0.03 (12)	0.75 (9)	0.81 (13)	0.79 (9)	0.79 (9)
U_{23}	0.75 (9)	0.91 (9)	1.05 (13)	0.92 (10)	0.76 (15)	0.74 (9)	0.75 (9)
O2							
U_{11}	0.56 (10)	0.60 (9)	0.41 (15)	0.57 (10)	0.52 (16)	0.60 (10)	0.56 (10)
U_{22}	2.21 (13)	2.39 (13)	1.65 (19)	2.36 (13)	2.20 (21)	2.26 (13)	2.21 (13)
U_{33}	1.61 (13)	1.46 (12)	0.62 (17)	1.45 (13)	1.47 (22)	1.65 (13)	1.61 (13)
U_{12}	0.38 (11)	0.44 (10)	0.09 (14)	0.47 (10)	0.61 (20)	0.40 (11)	0.38 (11)
U_{13}	0.60 (10)	0.50 (9)	0.50 (14)	0.49 (10)	0.56 (16)	0.63 (10)	0.60 (10)
U_{23}	0.64 (10)	0.47 (9)	−0.32 (12)	0.48 (10)	0.89 (17)	0.62 (10)	0.64 (10)
O(H_2O)							
U_{11}	2.22 (14)	2.43 (13)	1.02 (16)	2.44 (14)	2.22 (23)	2.29 (14)	2.22 (14)
U_{22}	2.50 (18)	3.06 (18)	2.37 (25)	2.95 (19)	2.28 (32)	2.46 (18)	2.50 (18)
U_{33}	1.28 (15)	1.56 (14)	1.04 (21)	1.55 (15)	1.34 (26)	1.32 (14)	1.28 (15)
U_{12}	0.66 (14)	−0.29 (13)	0.10 (19)	−0.25 (13)	1.29 (25)	0.66 (14)	0.66 (14)
U_{13}	0.71 (12)	1.04 (12)	0.52 (16)	1.05 (13)	0.75 (21)	0.74 (12)	0.71 (12)
U_{23}	0.18 (12)	−0.62 (11)	−1.78 (18)	−0.61 (12)	0.96 (22)	0.19 (12)	0.18 (12)
H1							
U_{11}	3.24 (24)	4.23 (24)	2.35 (31)	4.16 (26)	2.7 (4)	3.24 (24)	3.25 (24)
U_{22}	3.96 (33)	3.90 (34)	4.9 (6)	3.83 (36)	3.9 (5)	3.93 (32)	3.95 (33)
U_{33}	1.04 (20)	2.29 (22)	2.18 (35)	2.23 (23)	0.16 (35)	1.07 (20)	1.04 (20)
U_{12}	0.08 (22)	0.14 (22)	1.16 (32)	0.14 (24)	−0.06 (33)	0.09 (21)	0.09 (22)
U_{13}	0.17 (20)	1.47 (21)	1.30 (31)	1.44 (22)	−0.60 (33)	0.21 (20)	0.17 (20)
U_{23}	0.24 (22)	0.12 (22)	1.22 (31)	0.09 (23)	0.0 (4)	0.22 (21)	0.24 (22)
H2							
U_{11}	3.96 (27)	4.42 (28)	2.70 (35)	4.41 (30)	4.4 (5)	4.02 (27)	3.96 (27)
U_{22}	3.81 (33)	3.76 (31)	3.5 (4)	3.63 (33)	3.9 (5)	3.80 (32)	3.82 (33)
U_{33}	3.81 (28)	2.99 (24)	0.54 (24)	2.99 (25)	4.5 (4)	3.86 (28)	3.81 (28)
U_{12}	0.00 (32)	−0.41 (28)	−3.62 (36)	−0.32 (29)	0.1 (6)	0.05 (31)	0.00 (32)
U_{13}	1.86 (26)	1.35 (23)	−0.78 (26)	1.33 (24)	2.85 (46)	1.92 (26)	1.86 (26)
U_{23}	−0.99 (30)	−1.12 (25)	−0.51 (32)	−1.07 (27)	−0.7 (6)	−0.99 (30)	−1.00 (30)

Table 6
Bond lengths (Å) and angle (°) of the water molecule in gypsum from the Rietveld refinements to investigate the effect of the choice and level of the background on the extracted parameters.

A description of each set of refinements is given in the text.

Bond/angle	(1)	(2)	(3)	(4)	(5)	(6)	(7)
O—H1	1.007 (6)	0.987 (7)	0.976 (9)	0.987 (7)	1.022 (9)	1.007 (6)	1.007 (6)
O—H2	0.929 (7)	0.938 (7)	0.868 (10)	0.945 (7)	0.935 (11)	0.932 (7)	0.929 (7)
H1—O—H2	107.2 (5)	108.2 (5)	112.7 (7)	108.2 (5)	105.8 (7)	107.2 (5)	107.2 (5)

3.2.2. D20 detector stability and counting statistics saturation. The stability of the instrument as a function of data collection time was probed by following the refined scale factor obtained from the Rietveld refinements with no normalization applied for the incident monitor and the individual scale factors refined for the data sets. Fig. 6 shows the results for each of the sample can sizes for the 1.87 Å data. As can be readily seen, the linear fits as a function of time for each sample pass through, or very close to, zero. There is also no obvious deviation from linearity as a function of time for any of the sample sizes, particularly at shorter counting times, illustrating that the detector is very stable over a wide range of count rates with little or no change in the detection efficiency.

A further parameter of interest is the point at which the counting statistics become saturated, which can be described as the point where the systematic error contribution becomes the dominating component in the standard uncertainty determination in the Rietveld analysis, as described by Baharie & Pawley (1983) and Young (1996). The variation of the Rietveld agreement factors, the standard uncertainties and the overall goodness-of-fit index as a function of counting time and step size has been covered in detail previously (Hill & Madsen, 1984, 1986, 1987). In practice, what this means for data collection is that there comes a point after which continuing collection does not improve the information content of the data. For a fixed-step-width data collection this is manifested through the standard uncertainties of the refined variables tending to a finite value with increasing counting time. Fig. 7 shows the variation of the ratio of the standard uncertainty at time t to the standard uncertainty at $t_{\max}$ of the refined x position of atom H1 as a function of counting time for the largest (9 mm) and smallest samples (5 mm) so that the behaviours can be compared. For the 9 mm sample the standard uncertainties become effectively constant in around 50 min, *cf.* between 150 and 200 min for the same value of the ratio to be reached with the smaller 5 mm sample. Only the largest and smallest samples are illustrated in Fig. 7, but the intermediate sample sizes show behaviour between the two plotted curves. Similar behaviour is seen for all of the refined parameters as a function of data collection strategy and sample size. It is also evident that the improvement in the standard uncertainties is very steep at low counting times and that, for the large sample, the improvement is minimal after 15 min of total data collection. The importance of these short times for counting statistics saturation, even with the smallest sample measured, will become apparent in the following section.

3.2.3. Other ILL powder instruments. In order to investigate the suitability of using the other powder instruments at ILL to study hydrogenous materials, data were collected on the instruments D1A and D2B, as outlined previously. Fig. 8 shows the final Rietveld fit to the middle part of the detector (highest resolution) for a 4 h total data collection from the instrument D2B using an incident wavelength of 1.594 Å, and Fig. 9 shows the analogous data from D1A collected over 14 h using an incident wavelength of 1.909 Å. Table 7 shows a summary of the atomic positions and standard uncertainties from the multi-wavelength Rietveld refinements of each instrument compared with various data collection times using D20 for the same sample can, and Fig. 10 shows the Rietveld fits of the high Q region of the data sets presented in Table 7.

It is clear from the table that the lowest standard uncertainties are obtained from D20 over longer counting times, even though the longest counting time for the sample on D20 was less than half that used on D2B and almost ten times less than that on D1A, and comparable standard uncertainties were obtained with data collections on D20 of 5 and 10 min duration. Taking into account the evolution of the standard uncertainties with counting time, as illustrated in Fig. 7, it is clear that data collection times on the other instruments would need to be at least five times longer in order to reach the saturation point given in the previous section for the 9 mm sample, giving around 24 h of data collection on D2B and 3–4 d for similar data statistics on D1A per neutron wavelength. While the absolute differences in the standard uncertainties may seem small, gypsum is a very simple case with only moderate hydrogen content and a small unit cell. In addition, the limited choice of wavelengths available at D1A and D2B means that the possibilities for tuning the instrument

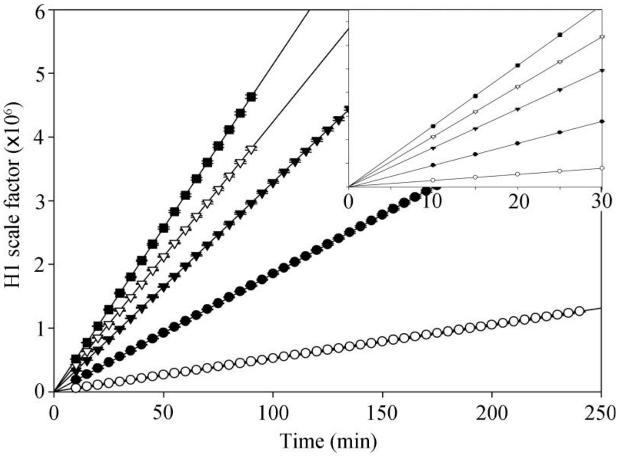

Figure 6
The refined scale factor as a function of counting time where the open circles are the 5 mm sample data, closed circles the 6 mm data, closed triangles the 7 mm data, open triangles the 8 mm data and closed squares the 9 mm data. The inset shows the low counting time region in each case. Where not visible, the error bars are within the size of the plotted points.

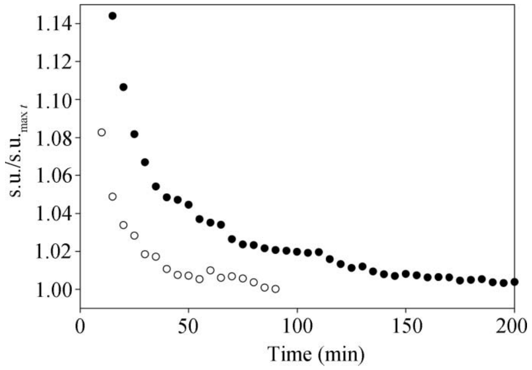

Figure 7
Plot of the variation of the ratio of the standard uncertainty to that at $t_{\max}$ (t = 90 min in the case of the 9 mm sample and t = 240 min for the 5 mm sample) of the x position of H1 as a function of counting time for the 5 mm sample (closed circles) and the 9 mm sample (open circles).

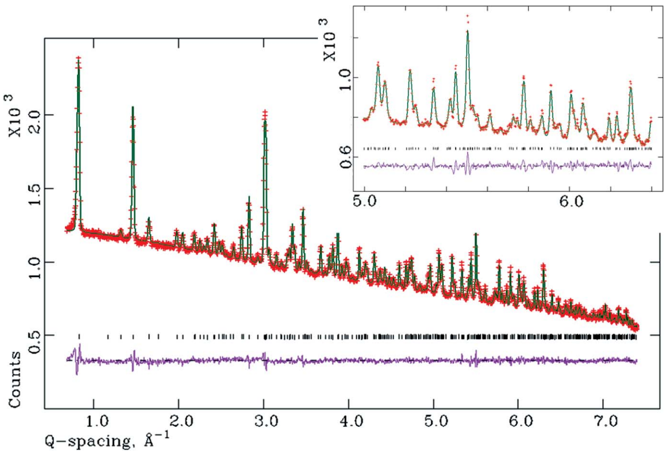

Figure 8
Final Rietveld refinement profile for the 1.594 Å incident wavelength data for the 9 mm sample can of gypsum on D2B. The observed data are crosses, the calculated pattern is a solid line, the tick marks show the allowed reflections and the lower solid line is the difference plot; $R_{\rm wp}$ = 1.42%, $R_{\rm p}$ = 1.08% and R_{F^2} = 9.15% for 438 observations. The inset shows the higher Q space region.

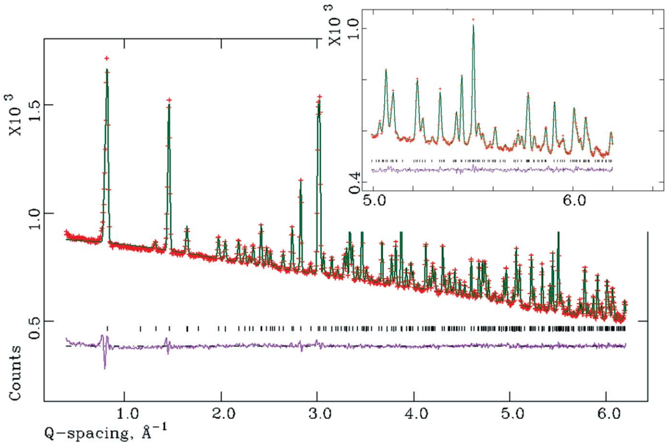

Figure 9
Final Rietveld refinement profile for the 1.909 Å incident wavelength data for the 9 mm sample can of gypsum on D1A. The observed data are crosses, the calculated pattern is a solid line, the tick marks show the allowed reflections and the lower solid line is the difference plot; $R_{\rm wp}$ = 1.08%, $R_{\rm p}$ = 0.77% and R_{F^2} = 4.78% for 254 observations. The inset shows the higher Q space region.

flux-resolution–spatial-range characteristics to the sample under investigation are limited compared with the situation for D20. Increasing the hydrogen content or the unit-cell complexity would quickly make the use of any instrument in the ILL powder diffraction suite except D20 prohibitively time consuming.

A further fact to note from Fig. 10 is the count rate from each instrument. A typical 300 s data set from D20 has over 2.1×10^4 counts on the Bragg reflection around 5.78 Å^{-1} compared with 1×10^3 (middle detector) and 3×10^3 (full detector) counts for D2B and 750 counts for D1A. Once the correction for the number of step scans required to obtain the full diffraction pattern is taken into account for the D2B and D1A data sets, these values become 8×10^3 and 2.4×10^4 counts, respectively, for D2B and 6×10^3 for D1A. The advantage of D20 lies in the fact that the area detector collects data in real time at all scattering angles where there is a detector (1536 detectors for D20 at 0.1° spacing), whereas the data from D1A and D2B per scattering angle are obtained over a significantly shorter time interval owing to the necessity

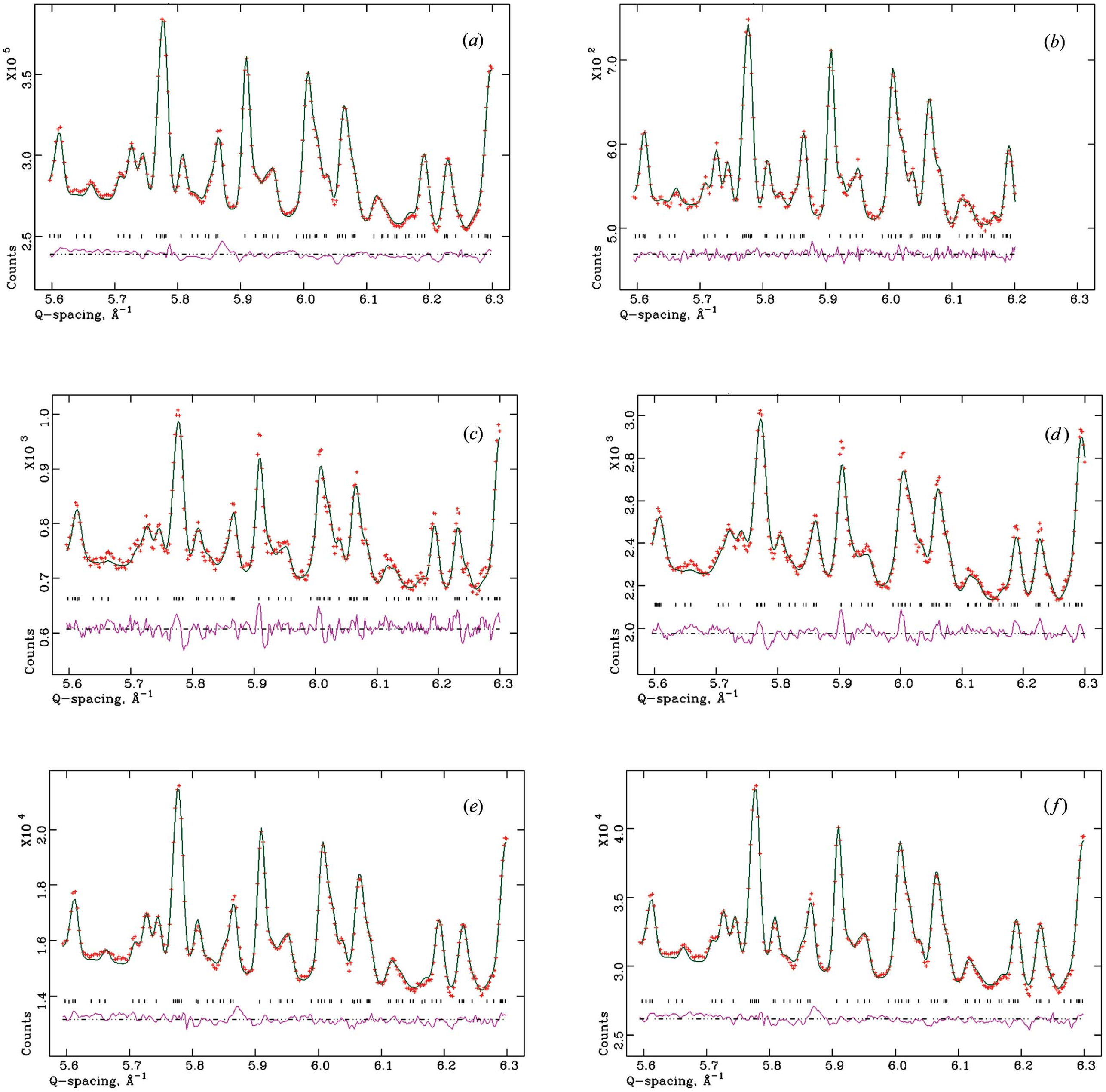

Figure 10

Rietveld refinement fits of the high Q region data for the results presented in Table 7. The observed data are crosses, the calculated patterns are solid lines, the tick marks show the allowed reflections and the lower solid lines are the difference plots, where (*a*) is a 90 min data collection on D20; (*b*) is a 14 h data collection on D1A; (*c*) is a 4 h data collection on D2B using only the middle part of the detector when summing (high resolution); (*d*) is the fit to the same data summed over the whole detector; (*e*) is a 300 s data collection on D20; and (*f*) is a 600 s data collection on D20.

Table 7
Refined atomic positions for gypsum for the different instruments at ILL.

	D20			D1A	D2B	
					Full detector	Middle only
Atom	90 min	5 min	10 min	14 h	4 h	4 h
Ca						
x	0.5	0.5	0.5	0.5	0.5	0.5
y	0.07872 (29)	0.07868 (34)	0.07909 (31)	0.07972 (31)	0.07928 (35)	0.0805 (4)
z	0.25	0.25	0.25	0.25	0.25	0.25
S						
x	0.0	0.0	0.0	0.0	0.0	0.0
y	0.0775 (4)	0.0774 (5)	0.0772 (4)	0.0765 (4)	0.0751 (5)	0.0762 (5)
z	0.75	0.75	0.75	0.75	0.75	0.75
O1						
x	0.9649 (4)	0.9648 (5)	0.9647 (5)	0.9643 (5)	0.9651 (5)	0.9648 (6)
y	0.13261 (16)	0.13261 (18)	0.13255 (17)	0.13235 (17)	0.13215 (19)	0.13169 (22)
z	0.5519 (4)	0.5523 (4)	0.5520 (4)	0.5512 (4)	0.5495 (4)	0.5502 (5)
O2						
x	0.7572 (4)	0.7573 (5)	0.7571 (5)	0.7578 (5)	0.7578 (5)	0.7571 (6)
y	0.02286 (17)	0.02292 (19)	0.02284 (18)	0.02181 (18)	0.02153 (20)	0.02224 (23)
z	0.6674 (4)	0.6673 (4)	0.6673 (4)	0.6675 (4)	0.6670 (5)	0.6668 (6)
O(H_2O)						
x	0.3808 (6)	0.3815 (7)	0.3811 (6)	0.3805 (6)	0.3799 (6)	0.3792 (9)
y	0.18264 (20)	0.18270 (23)	0.18265 (21)	0.18262 (31)	0.18225 (22)	0.18243 (29)
z	0.4569 (5)	0.4568 (6)	0.4571 (5)	0.4577 (5)	0.4578 (6)	0.4575 (7)
H1						
x	0.2486 (9)	0.2494 (11)	0.2493 (10)	0.2487 (10)	0.2501 (11)	0.2529 (15)
y	0.15985 (28)	0.16029 (33)	0.15988 (30)	0.16041 (30)	0.1602 (4)	0.1607 (4)
z	0.5068 (9)	0.5075 (10)	0.5073 (9)	0.5053 (9)	0.5004 (11)	0.5038 (13)
H2						
x	0.4067 (10)	0.4085 (12)	0.4076 (11)	0.4058 (11)	0.4063 (13)	0.4083 (15)
y	0.24186 (37)	0.24174 (44)	0.24197 (40)	0.24192 (39)	0.2428 (4)	0.2415 (5)
z	0.4937 (10)	0.4946 (12)	0.4939 (11)	0.4933 (11)	0.4905 (13)	0.4940 (15)

to step [see Hansen *et al.* (2008) for a discussion on relative data collection speed]. The effect of the step size on the derived standard uncertainties has not been taken into account in this manuscript, although it would be small as the step size for D1A and D2B is only half that of D20 (0.05 and 0.1°, respectively) and the FWHMs are not instrument-resolution limited in the case of gypsum. This can also been seen in Fig. 10 as there are at least four points over the FWHM of each of the Bragg reflections in patterns (*a*), (*e*) and (*f*) from D20, which is close to the suggested optimum of three–five. Accounts of the effect of step size on the derived standard uncertainties in a Rietveld refinement can be found in the work of Bérar & Lelann (1991) and Young (1996).

4. Discussion

D20 is clearly a class apart from the rest of the suite at ILL as a result of the tunability of the incident wavelength, Q range and flux on the sample to the system under investigation, and the high detector stability under variable count rate regimes, its efficiency and the scattering angle coverage with good angular resolution. For a typical sample size used in neutron powder diffraction (several cm^3) the average data collection times range from minutes to a few hours. The use of D1A and D2B for hydrogen-containing materials is likely to be limited to systems containing low levels of hydrogen with relatively small unit cells or materials where a need for very high detector resolution becomes the dominant factor in the choice of instrument, irrespective of the much longer counting times required. However, the justification for experiments requiring such long counting times becomes increasingly difficult and there are relatively few examples of nondeuterated systems studied using D1A or D2B without the necessity of deuteration (*e.g.* Ahmed *et al.*, 2008).

The instrument characteristics of D20 mean that there are also limitations to the types of materials that can be studied. Gypsum has a relatively simple structure with only five independent atomic positions and moderate hydrogen content. For crystallographically complex materials with very large unit cells (such as many organometallics, some metal–organic frameworks and large-molecule organic compounds) peak overlap in the powder diffraction pattern can be severe using thermal neutron wavelengths. Without higher detector resolution and beam collimation (that reduces the flux on the sample), the structural information embedded in the profile peak intensities cannot be readily accessed, or accessing it may require additional information or constraints (such as a combined refinement using a single-crystal X-ray diffraction data set or the use of rigid bodies or bond-distance/angle constraints). Therefore, the instrumental resolution effectively limits the size of the unit cells that can be refined. Our work on this subject is continuing across a range of systems (*e.g.* Henry *et al.*, 2008; Martins *et al.*, 2009; Weller *et al.*, 2009) and our results show that asymmetric unit cells with volumes up to ~800 Å^3 and up to 20 independent atom positions are readily studied. Our investigations to date show that the hydrogen content of the material does not seem to be a factor in limiting this type of work; although for a higher hydrogen content, longer data collection times are required to achieve adequate peak-to-noise ratios, the collection times remain of the order of hours rather than days. By combining the data with single-crystal X-ray data sets or through the use of bond-length constraints and rigid bodies, much more complex systems can be studied (with typically 50+ atoms in the asymmetric unit cells), even with high hydrogen content.

5. Conclusion

We have demonstrated that neutron powder diffraction from high-flux constant-wavelength sources can be a valuable tool for the routine study of hydrogenous materials without the necessity to deuterate the sample. For modern constant-wavelength instrumentation like D20, count times to obtain high-quality diffraction data for full-profile analysis using the Rietveld method can be reduced from days to between minutes and a few hours. Further developments in neutron diffraction instrumentation and detector technology of constant-wavelength diffraction instruments will lead to further advances in this area, especially in terms of the crystallographic complexity of materials that can be studied. While some factors affecting data quality remain to be fully quantified, such as packing density, chemical environment and the effect of the variation of the incoherent scattering cross section of hydrogen with wavelength (see Howard *et al.*, 1987; Koetzle & Mcmullan, 1980; Frost, 1989), it is clear that the method has a sound scientific basis as shown by the increasing number of published results. The potential is enormous given the extensive range of hydrogen-containing compounds and their importance in materials chemistry, geochemistry and life sciences and as energy materials.

We would like to thank the Institut Laue–Langevin for granting beamtime contributing to this work under the proposal numbers 5-24-248 and 5-26-187. We would also like to thank the EPSRC for funding the work through grants EP/E051049/1 and EP/E050859/1.

References

Ahmed, I., Knee, C. S., Karlsson, M., Eriksson, S. G., Henry, P. F., Matic, A., Engberg, D. & Börjesson, L. (2008). *J. Alloys Compd.* **450**, 103–110.

Atoji, M. & Rundle, R. E. (1958). *J. Chem. Phys.* **29**, 1306–1311.

Baharie, E. & Pawley, G. S. (1983). *J. Appl. Cryst.* **16**, 404–406.

Belsky, A., Hellenbrandt, M., Karen, V. L. & Luksch, P. (2002). *Acta Cryst.* B**58**, 364–369.

Bérar, J.-F. & Lelann, P. (1991). *J. Appl. Cryst.* **24**, 1–5.

Berenblut, B. J., Dawson, P. & Wilkinson, G. R. (1974). *Spectrochim. Acta Part A*, **29**, 29–36.

Bergerhoff, G. & Brown, I. D. (1987). *Crystallographic Databases*, by F. H. Allen, G. Bergerhoff & R. Sievers. Chester: International Union of Crystallography.

Boeyens, J. C. A. & Ichharam, V. V. H. (2002). *Z. Kristallogr.* **217**, 9–10.

Cicognani, G. (2005). Editor. *The Yellow Book*. Grenoble: Institut Laue–Langevin. Online version at http://www.ill.eu/instruments-support/instruments-groups/yellowbook/.

Cole, W. F. & Lancucki, C. J. (1974). *Acta Cryst.* B**30**, 921–929.

Convert, P., Hansen, T., Oed, A. & Torregrossa, J. (1998). *Physica B*, **241–243**, 195–197.

Convert, P., Hansen, T. & Torregrossa, J. (2000). *Mater. Sci. Forum*, **321–324**, 314–319.

Frost, C. D. (1989). ILL Internal Report. Institut Laue–Langevin, Grenoble, France.

Hansen, T. C. (2004). *Mater. Sci. Forum*, **443–444**, 181–186.

Hansen, T. C., Henry, P. F., Fischer, H. E., Torregrossa, J. & Convert, P. (2008). *Meas. Sci. Technol.* **19**, 034001.

Henry, P. F., Weller, M. T. & Wilson, C. C. (2008). *Chem. Commun.* pp. 1557–1559.

Hill, R. J. & Madsen, I. C. (1984). *J. Appl. Cryst.* **17**, 297–306.

Hill, R. J. & Madsen, I. C. (1986). *J. Appl. Cryst.* **19**, 10–18.

Hill, R. J. & Madsen, I. C. (1987). *Powder Diffr.* **2**, 146–162.

Howard, J. A. K., Johnson, O., Schultz, A. J. & Stringer, A. M. (1987). *J. Appl. Cryst.* **20**, 120–122.

Krishnamurthy, N. & Soots, V. (1971). *Can. J. Phys.* **49**, 885–896.

Koetzle, T. F. & McMullan, R. K. (1980). Research Memo C-4. Brookhaven National Laboratory, Upton, New York, USA.

Kuhs, W. (2008). Unpublished work from ILL experiment No. 5-25-150. Institut Laue–Langevin, Grenoble, France.

Langford, J. L. & Louer, D. (1996). *Rep. Prog. Phys.* **59**, 131–234.

Larson, A. C. & Von Dreele, R. B. (1994). *General Structure Analysis System* (*GSAS*). Report LAUR 86-748. Los Alamos National Laboratory, New Mexico, USA.

Martins, D. M. S., Middlemiss, D. S., Pulham, C. R., Wilson, C. C., Weller, M. T., Henry, P. F., Shankland, N., Shankland, K., Marshall, W. G., Ibberson, R. M., Moggach, S., Brunelli, M. & Morrison, C. A. (2009). *J. Am. Chem. Soc.* **131**, 3884–3893.

Pedersen, B. F. & Semmingsen, D. (1982). *Acta Cryst.* B**38**, 1074–1077.

Richard, D., Ferrand, M. & Kearley, G. J. (1996). *J. Neutron Res.* **4**, 33–39.

Rouse, K. D., Cooper, M. J., York, E. J. & Chakera, A. (1970). *Acta Cryst.* A**26**, 682–691.

Schmitt, D. & Ouladdiaf, B. (1998). *J. Appl. Cryst.* **31**, 620–624.

Schofield, P. F., Knight, K. S. & Stretton, I. C. (1996). *Am. Mineral.* **81**, 847–851.

Schofield, P. F., Wilson, C. C., Knight, K. S. & Stretton, I. C. (2000). *Z. Kristallogr.* **215**, 707–710.

Seidl, V., Knop, O. & Falk, M. (1969). *Can. J. Chem.* **47**, 1361–1368.

Toby, B. H. (2001). *J. Appl. Cryst.* **34**, 210–213.

Weller, M. T., Henry, P. F., Ting, V. P. & Wilson, C. C. (2009). *Chem. Commun.* pp. 2973–2989.

Winkler, B. & Hennion, B. (1994). *Phys. Chem. Miner.* **21**, 539–545.

Wooster, W. A. (1936). *Z. Kristallogr.* **94**, 375–396.

Young, R. A. (1996). Editor. *The Rietveld Method*, ch. 5. New York: Oxford University Press.